Imaging Quantum Interference in a Monolayer Kitaev Quantum Spin Liquid Candidate

Y. Kohsaka,[1,*] S. Akutagawa,[1] S. Omachi,[1] Y. Iwamichi,[1] T. Ono,[1,2] I. Tanaka,[1] S. Tateishi,[1] H. Murayama,[1,3] S. Suetsugu,[1] K. Hashimoto,[2] T. Shibauchi,[2] M. O. Takahashi,[4] S. Nikolaev,[4] T. Mizushima,[4] S. Fujimoto,[4] T. Terashima,[1] T. Asaba,[1] Y. Kasahara,[1] and Y. Matsuda[1,†]

[1]*Department of Physics, Kyoto University, Kyoto 606-8502, Japan*
[2]*Department of Advanced Materials Science, University of Tokyo, Kashiwa, Chiba 277-8561, Japan*
[3]*RIKEN Center for Emergent Matter Science, Wako, Saitama 351-0198, Japan*
[4]*Department of Materials Engineering Science, Osaka University, Toyonaka 560-8531, Japan*

(Received 25 March 2024; revised 4 September 2024; accepted 17 September 2024; published 25 October 2024)

Single atomic defects are prominent windows to look into host quantum states because collective responses from the host states emerge as localized states around the defects. Friedel oscillations and Kondo clouds in Fermi liquids are quintessential examples. However, the situation is quite different for quantum spin liquid (QSL), an exotic state of matter with fractionalized quasiparticles and topological order arising from a profound impact of quantum entanglement. Elucidating the underlying local electronic property has been challenging due to the charge neutrality of fractionalized quasiparticles and the insulating nature of QSLs. Here, using spectroscopic-imaging scanning tunneling microscopy, we report atomically resolved images of monolayer α-$RuCl_3$, the most promising Kitaev QSL candidate, on metallic substrates. We find quantum interference in the insulator manifesting as incommensurate and decaying spatial oscillations of the local density of states around defects with a characteristic bias dependence. The oscillation differs from any known spatial structures in its nature and does not exist in other Mott insulators, implying it is an exotic oscillation involved with excitations unique to α-$RuCl_3$. Numerical simulations suggest that the observed oscillation can be reproduced by assuming that itinerant Majorana fermions of Kitaev QSL are scattered across the Majorana Fermi surface. The oscillation provides a new approach to exploring Kitaev QSLs through the local response against defects like Friedel oscillations in metals.

DOI: 10.1103/PhysRevX.14.041026

Subject Areas: Condensed Matter Physics, Strongly Correlated Materials

I. INTRODUCTION

Uniform electronic states of matter rearrange themselves in response to defects, forming characteristic spatial structures. The local electronic structure around defects is thus a fundamental fingerprint reflecting low-energy excitations of the host state. Eminent examples are screening phenomena of metals: Friedel oscillations for charged defects and Kondo clouds for magnetic defects [1,2]. Advances in techniques of scanning tunneling microscopy allow us to directly image such defect states not only in metals but also in various quantum materials at atomic resolution unavailable by other means [3–5].

Utilizing defect states as *in situ* probes is envisioned to search for quantum spin liquid (QSL), a highly entangled quantum-disordered state of insulating frustrated magnets [6–13]. Depending on the symmetry of the system, several types of QSLs and accompanying fractionalized quasiparticles are predicted [6]. Among the QSLs is the Kitaev QSL, which has sparked an explosion of research because of Majorana fermions and non-Abelian anyons resulting from the fractionalization of the quantum spin [6,14–16]. The Kitaev model formulates localized $s = 1/2$ spins on a two-dimensional (2D) honeycomb lattice interacting through bond-dependent Ising couplings. It is noteworthy that it possesses an exactly solvable ground state, from which Majorana fermions naturally emerge. This aspect is distinct from the unresolved ground states of triangular and kagome QSL candidate systems. Following the seminal proposal to embody the Kitaev model [17], a spin-orbit Mott insulator α-$RuCl_3$ was suggested as a promising candidate [18–21]. Since then, a growing body of evidence has been accumulated to indicate the presence of Majorana fermions at low energies in this compound by

*Contact author: kohsaka.yuhki.3j@kyoto-u.ac.jp
†Contact author: matsuda@scphys.kyoto-u.ac.jp

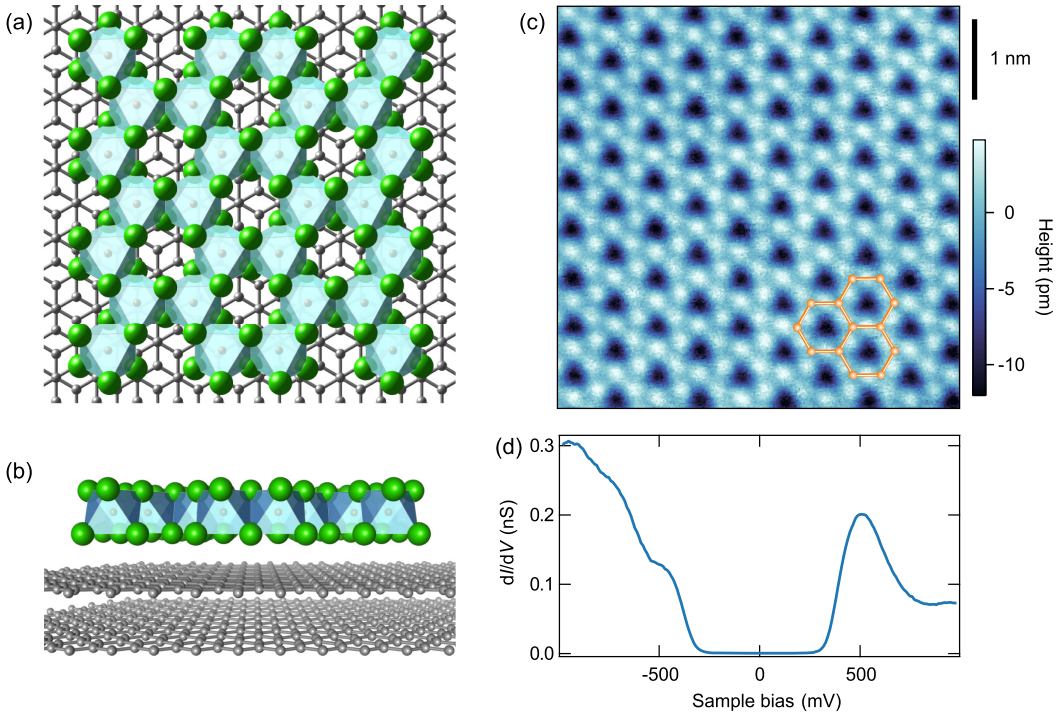

FIG. 1. A monolayer α-$RuCl_3$ film fabricated on a graphite substrate. (a),(b) Illustrations of a monolayer α-$RuCl_3$ film grown on a graphite substrate, drawn using VESTA [47]. Panels (a) and (b) are seen from (001) and (100) directions of the monolayer α-$RuCl_3$ film, respectively. The relative angle between the α-$RuCl_3$ lattice and the graphite lattice drawn in the illustrations differs from the actual angles. (c) A topographic image of a monolayer α-$RuCl_3$ film. The setpoint condition is +1 V and 0.2 nA. The overlaid illustration depicts the position of the Ru honeycomb. (d) A typical conductance spectrum. The setpoint condition is +0.98 V and 0.2 nA.

measurements of Raman scattering, inelastic neutron scattering, specific heat, and thermal Hall effect [22–32]. Despite such extensive studies, there is still room for debate on whether the Kitaev QSL is realized in α-$RuCl_3$ [33].

The quest for QSLs, including the Kitaev QSL, has been driven by spatially averaged probes, as exemplified above. Consequently, the experimental data and their interpretations have often been influenced by undesirable complexities due to structural disorders such as stacking faults and antisite defects [21,34]. Using spatially resolved probes on thin films is a reasonable way to circumvent these issues. Additionally, for α-$RuCl_3$, thin film samples can serve as an alternative to applying a horizontal magnetic field to suppress the zigzag antiferromagnetism, which is a three-dimensional order [35]. Furthermore, beyond the general context to investigate defect states described above, local electronic probes have been theoretically proposed to detect and control fractional magnetic excitations [36–41]. These previous studies underscore the need for scanning tunneling microscopy of monolayer thin films. Recently, monolayer 1*T*-$TaSe_2$, a candidate for another QSL in a 2D triangular lattice Mott insulator, has been examined by a scanning tunneling microscope (STM) [42,43]. These pioneering works have suggested that the low-energy magnetic excitations could be detected experimentally at higher energies outside the Mott gap by measuring the tunneling electrons recombined from the fractionalized quasiparticles, called spinons. Raman scattering study of exfoliated monolayer films of α-$RuCl_3$ uncovered enhanced frustrated magnetic interactions and the unusual magnetic continuum indicating proximate QSL in the 2D samples [44]. However, atomically resolved STM studies revealed that exfoliated samples can be deformed and exhibit highly inhomogeneous spectra [45,46]. These results highlight the need for STM measurements on thin films fabricated in a more controlled manner. We therefore fabricated monolayer α-$RuCl_3$ films on highly oriented pyrolytic graphite (HOPG) substrates by pulsed laser deposition [Figs. 1(a) and 1(b)] and conducted the electronic imaging study using an STM. (See Sec. IV for details.)

II. RESULTS

We first inspect fabricated films. Figure 1(c) shows an atomic-resolution topographic image of our film. Regularly arranged circular protrusions form a kagomelike lattice, replicating the previous study of monolayer α-$RuCl_3$ [48]. The protrusions are primarily ascribed to derive from the topmost Cl *p* orbitals, with the Ru site residing at the center of three protrusions. Because of the hybridization of Cl *p*

and Ru d orbitals, the center of the protrusion slightly shifts from the Cl site toward the Ru site, resulting in the kagomelike lattice [48]. A Ru honeycomb encloses a dark-colored hollow site, as shown in the overlaid illustration of Fig. 1(c). The conductance spectrum exemplified in Fig. 1(d) is also similar to the previous study. It shows an energy gap of about 0.6 eV with the Fermi energy in the middle of the gap, indicating that the sample is an insulator. The apparent film thickness is also very close to the value in Ref. [48]. (See Supplemental Material A. Statistical analysis of apparent film thickness for details [49].) From these close similarities with the previous study, we identify that the films are monolayer α-$RuCl_3$.

Our spectra are strikingly different from the metallic spectra of the exfoliated films [45,46,57], indicating that our samples are unaffected by the lattice deformation. Furthermore, the Fermi energy in the middle of the gap does not align with sizable electron transfer from the HOPG substrate observed in some experiments [58–60]. We note that the samples in these experiments are also prepared by exfoliation. Practically, the properties of insulators or metals can vary depending on the fabrication methods: deposition and epitaxy, or exfoliation. In our case, the weak coupling between the α-$RuCl_3$ film and the HOPG substrate, inferred from the apparent film thickness and the random orientation (described below), may be preventing electron transfer and thus keeping the sample insulating.

We next focus on the most peculiar feature we have observed. Figures 2(b) and 2(a) are topographic images taken at $+1$ V in the same field of view. We find concentric oscillatory patterns around defects. High-resolution measurements allow us to identify several types of defects (Fig. S1 in Supplemental Material [49]), showing that the oscillation appears independently of the defect sites. The oscillation is several times larger in amplitude at -1 V than at $+1$ V and decays away from the defects, as highlighted in Figs. 2(c) and 2(d) (see also Fig. S2 [49]). The local amplitude maps of the oscillation, as depicted in Figs. 2(e) and 2(f), further demonstrate that the oscillation is localized around the defects and diminishes with increasing distance from them. The decay means that the oscillation is not a moiré pattern between the monolayer α-$RuCl_3$ and the substrate.

To analyze the wave vectors of oscillation, we calculated the Fourier transform, as shown in Figs. 3(a) and 3(b). We suppressed long-wavelength features from the defects for clarity, as demonstrated in Fig. S3 in Supplemental Material [49]. Strong peaks corresponding to the oscillations, indicated by the pink ovals, are found roughly in the Γ-K direction. The wave numbers of the oscillation are incommensurate. (See also Supplemental Material C for more details [49].) More critically, they differ between the $+1$ V images, as shown in Fig. 3(c). In contrast, the wave vectors of the lattice peaks are

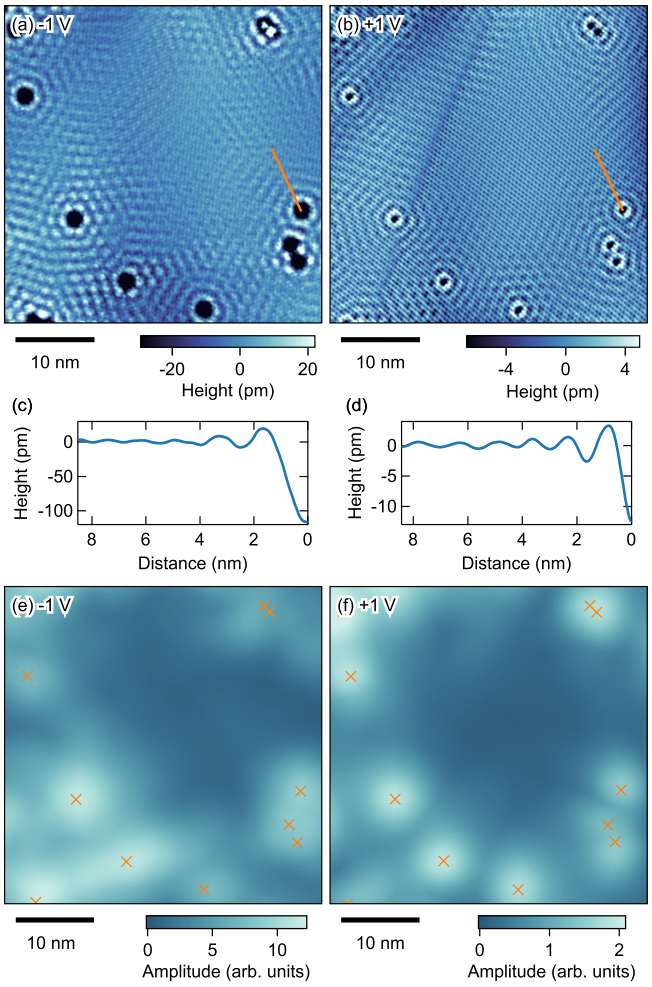

FIG. 2. Spatial oscillation of the local density of states decaying away from defects. (a),(b) Topographic images of an α-$RuCl_3$ monolayer film taken at -1 V and 0.25 nA for (a) and $+1$ V and 0.5 nA for (b). The orange lines denote the positions of the line profiles in (c) and (d). (c),(d) The line profiles obtained from the low-pass filtered images shown in Fig. S2 in Supplemental Material [49] along the trajectories shown in (a) and (b), respectively. (e),(f) The local amplitude maps of the oscillation in the same field of view as (a) and (b), respectively. The orange markers are placed at the defect centers. The calculation of the local amplitude map is described in Supplemental Material B. Local amplitude map of the decaying oscillation [49].

independent of the bias voltage, as shown in Fig. 3(d). Similarly, the peak positions of charge density waves do not depend on the bias voltage for the same reason [42]. Namely, the wave numbers different between $+1$ V indicate that the origin of the incommensurate oscillation is electronic rather than structural. Consequently, we exclude phenomena involving lattice distortion, such as charge density waves and local strains, as the origin of the oscillation. In addition, due to the decaying feature and the different wave numbers, the oscillation is distinguished from the long-wavelength supermodulations in monolayer

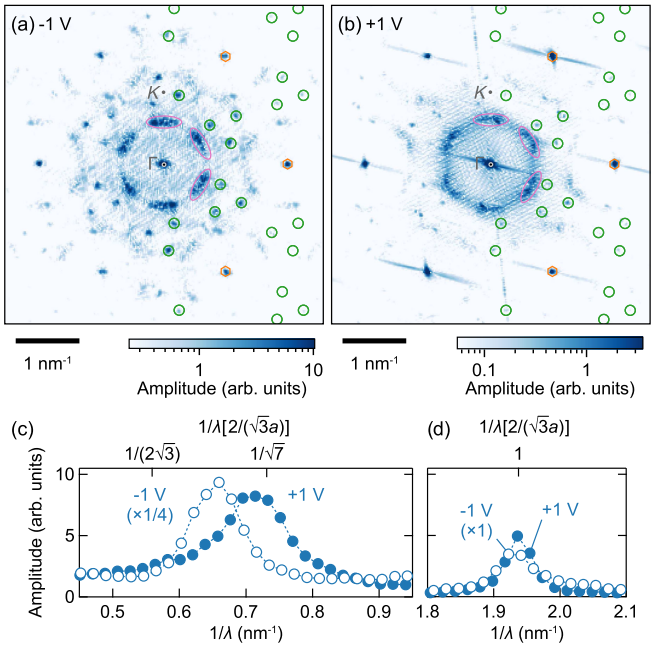

FIG. 3. (a),(b) Fourier transforms of images including Figs. 2(a) and 2(b), respectively. The images are 54×43 nm^2 for (a) and 54×54 nm^2 for (b). The pink ovals indicate the peaks corresponding to the oscillation decaying away from the defects. The orange hexagons and the green circles denote the positions of the α-$RuCl_3$ lattice peaks and the satellite peaks, respectively. The satellite peak positions are calculated as described in Supplemental Material D with an angle of 31° [49]. The markers are shown only in the right-hand half of each panel. The defects in (a) are masked before calculating (a) to suppress large intensity around the origin, as shown in Fig. S3 [49]. (c),(d) The azimuthal averages of (a) and (b). The top axis is shown in units of the inverse of the lattice constant. The vertical axis range is common to (c) and (d).

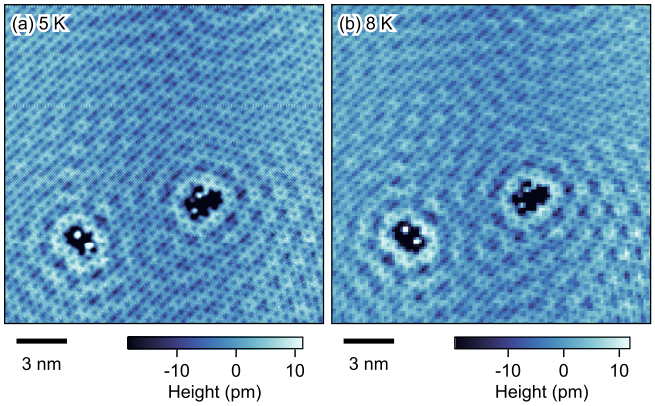

FIG. 4. Comparison of topographic images taken at 5 and 8 K. Both images were taken in the same field of view of 19×19 nm^2 and at a setpoint condition of +0.98 V and 0.1 nA.

$1T$-$TaSe_2$ [42]. Interestingly, a similar pattern has been independently observed by another group [61]. There are both similarities and differences: The similarities include an apparent resemblance, especially at negative biases, and different wave numbers between the polarities; the differences include the presence of a decaying feature, incommensurate oscillations, and no apparent rotational symmetry breaking in our case.

The Fourier transforms also show many bias-independent peaks [the green circles in Figs. 3(a) and 3(b)] besides the lattice peaks [the orange hexagons Figs. 3(a) and 3(b)]. These are satellite peaks generated by the α-$RuCl_3$ lattice and the substrate HOPG lattice with a certain angle. (How to calculate the peak positions and the angle is described in Supplemental Material D [49].) We also found a monolayer α-$RuCl_3$ film with a different angle and observed the same oscillations (Fig. S4 [49]). The insensitivity to the relative angles demonstrates that the oscillation is irrelevant to coupling with the substrate. Moreover, electron tunneling directly from the substrate is negligibly small, as evidenced by the zero conductance in the insulating gap [Fig. 1(d)]. Therefore, the oscillation is inherent to the monolayer α-$RuCl_3$ and occurs in the monolayer α-$RuCl_3$, neither in the substrate nor at the interface between the monolayer α-$RuCl_3$ and the substrate.

Since the oscillation is electronic in origin and occurs in α-$RuCl_3$, one may wonder if the zigzag antiferromagnetic order found in the bulk α-$RuCl_3$ is relevant to the oscillation. The fact that the oscillation patterns are not unidirectional but approximate hexagonal shapes indicates that they are unrelated to the zigzag antiferromagnetic order. Furthermore, the temperature dependence of the pattern also supports the irrelevance. In the presence of the Kitaev interaction, the zigzag antiferromagnetic order arising from non-Kitaev interactions is indeed allowed even in 2D without being forbidden by the Mermin-Wagner theorem because the Kitaev interaction has Z_2 symmetry [62]. However, even if it exists, the Néel temperature is expected to be lower in 2D films than in the bulk since the zigzag antiferromagnetic order is three dimensional [35]. Moreover, the Imry-Ma argument indicates that long-range magnetic orders with Z_2 symmetry are destroyed in 2D by infinitesimally weak disorders [63]. Therefore, we presume that the zigzag antiferromagnetic order is absent at 8 K, higher than the Néel temperature of 7 K in the bulk. As shown in Fig. 4, a topographic image taken at 8 K shows no discernable difference from one at 5 K, indicating that the oscillation has nothing to do with the zigzag antiferromagnetic order.

The oscillatory patterns in the STM images (and also the conductance maps described later) decaying away from the defects imply quantum interference of fermionic quasiparticles around the defects. At first glance, the patterns resemble the Friedel oscillations in metals and quasiparticle interference. Although a straightforward case of Friedel oscillations is ruled out because the monolayer α-$RuCl_3$ is insulating, as evidenced by the energy gap [Fig. 1(d)], Friedel oscillations could

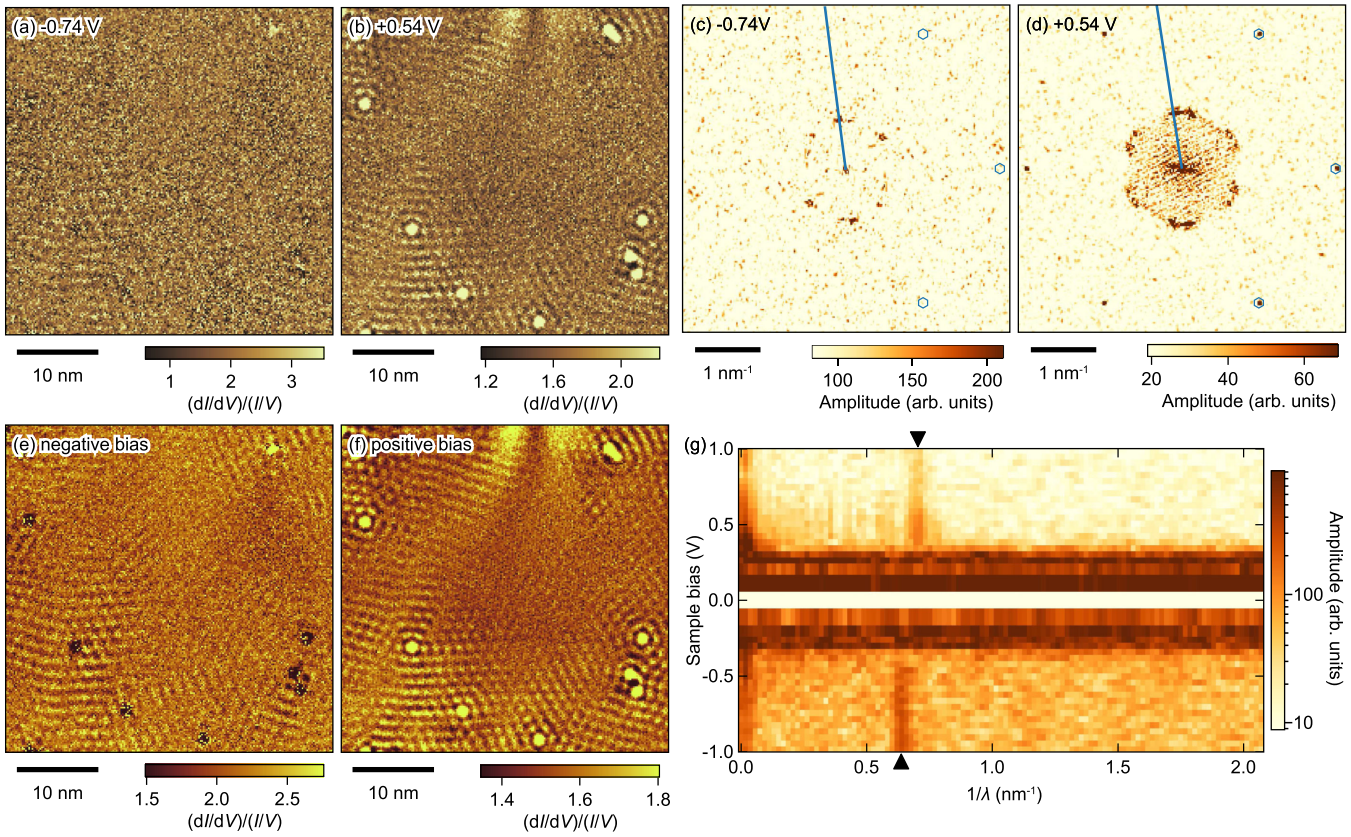

FIG. 5. The maps of normalized conductance $(\mathrm{d}I/\mathrm{d}V)/(I/V)$. (a),(b) The normalized conductance maps taken at -0.74 and $+0.54$ V, respectively, in the same field of view of Figs. 2(a) and 2(b). (c),(d) Fourier transforms of normalized conductance maps. The original images were measured in a 54×53 nm^2 field of view, including (a) and (b), with a setpoint condition of $+0.98$ V and 0.1 nA. The blue hexagons in the right-hand half of each panel denote the positions of the lattice peaks. (e),(f) The normalized conductance maps averaged between -1 and -0.42 V for (e) and $+0.42$ and $+1$ V for (f). The field of view is the same as (a) and (b). (g) Dispersion relation along the blue lines in (c) and (d). The triangle markers indicate the bias-semi-independent wave vectors of the oscillatory patterns.

potentially occur if the tip-induced band bending is sufficient to induce carriers. In this case, the oscillation period would depend on the density of induced carriers and the bias voltages. The wave vectors of quasiparticle interference, which reflect the band structure, also vary with the energy. Therefore, the dispersion relationship of the oscillation is crucial to explore these possibilities. Figure 5 displays the result of spectroscopic imaging we have performed to delineate the dispersion relation. We adopt the normalized conductance $[(\mathrm{d}I/\mathrm{d}V)/(I/V)]$ map [Figs. 5(a) and 5(b)] rather than the raw conductance $(\mathrm{d}I/\mathrm{d}V)$ map to mitigate the setpoint effect (Fig. S5 in Supplemental Material [49]). Figures 5(c) and 5(d) show Fourier transforms of conductance maps. Peaks corresponding to the oscillation are observed in the bias range outside the energy gap. Notably, the wave vectors differ between the polarities but do not change in each polarity, as shown in Fig. 5(g). The wave vector at each polarity is the same as that observed in the corresponding topographic image. Indeed, the normalized conductance images averaged for the negative and positive bias voltages [Figs. 5(e) and 5(f)] exhibit oscillations similar to those in the topographic images [Figs. 2(a) and 2(b)]. We refer to this behavior of the experimental data as semi-independent of the bias voltage. The bias-independent aspect indicates that the oscillation is neither Friedel oscillations by the induced carriers nor quasiparticle interference. We note that nondispersive quasiparticle interference, requiring electron bands to be parallelly shifted, results in vanishing interference intensity due to destructive interference [64].

III. DISCUSSION

As mentioned above, the observed patterns differ from the known phenomena producing oscillatory patterns, such as moiré, charge density waves, Friedel oscillations, quasiparticle interference, and the supermodulation in monolayer $1T$-$TaSe_2$ [42]. Therefore, we conclude that the observed oscillation is an unprecedented oscillatory phenomenon. Since the oscillation appears in the energy range of lower and upper Hubbard bands, one could assume that

the Hubbard interaction is involved in the oscillation. However, no other Mott insulators exhibit oscillations around defects [65–68]. Also, one might consider that the oscillation is special to monolayer films. However, the decaying and bias-semi-independent oscillation is not found in other insulating monolayer films [42,43,68–70]. Therefore, something unique to α-$RuCl_3$ is likely to be responsible for the oscillation.

Given that α-$RuCl_3$ is a promising candidate for Kitaev QSL, we might consider the Kitaev interaction as a possible origin of the oscillation. Then, two immediate questions arise: How are the spin properties amenable to detection using nonmagnetic scanning tips, and what determines the length scale of the incommensurate oscillation? For the former, if spin-charge separation occurs, the tunneling electrons recombined from spinons and chargons may carry spin information [13,42,43]. However, this process is not the case for the Kitaev QSL because fractionalization occurs solely in the spin system. Instead, we consider a relationship in the Mott insulator that the charge density is tied to the spin correlation function [36,71]. A spatial texture of the spin correlation function is then reflected in the charge density variation, which is readily imaged as a bias-independent pattern using an STM with a nonmagnetic scanning tip. For the length scale of the oscillation, the incommensurability of the oscillation hints at the scattering of itinerant quasiparticles with a characteristic length akin to a Fermi wavelength. In the Kitaev QSL, the spins are fractionalized into itinerant and localized Majorana fermions; the former move around the whole crystal, while the latter form a Z_2 vortex called vison [16]. Thus, itinerant Majorana fermions could play an essential role in the oscillation. However, for the pure Kitaev model, the scattering vectors of the itinerant Majorana fermions at the Fermi energy are commensurate because the Dirac points of the Majorana band cross the Fermi energy at K and K' points in the Brillouin zone. Nevertheless, the Majorana Fermi surface with incommensurate Fermi wave numbers is possibly realized if there are perturbations breaking time-reversal and inversion symmetries that protect the positions of the Dirac points [72,73]. Postulating that both symmetries are locally broken by the tunneling current injected from the scanning tip, the calculations of charge density variation reproduce the observed incommensurate oscillation, as shown in Fig. 6. In this scenario, the slightly different wave numbers depending on the bias polarities could be attributed to the fact that the correction to the Kitaev interaction due to the bias voltages is asymmetric with respect to the sign of the voltages. In fact, a negative bias potential imposed by the scanning tip may induce virtual processes with extra holes associated with the Kitaev interaction arising from the Hund coupling between the $j = 1/2$ and $j = 3/2$ states, which results in the increase of the Kitaev interaction as described by $\sim(t^2 J_H/U^2) + J_H(t/U)^2(t_S/U)^2$. Here, the

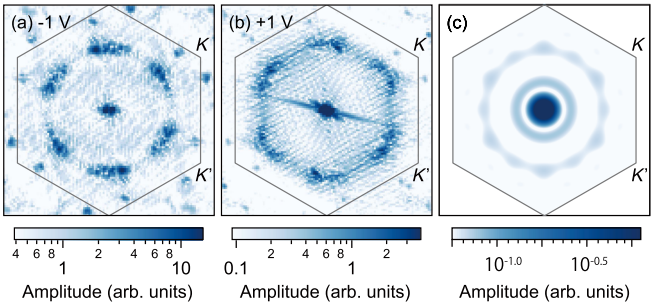

FIG. 6. Comparison between the experimental data and the numerical simulation. (a),(b) Fourier transforms of topographic images at −1 and +1 V, respectively. These are the central part of Figs. 3(a) and 3(b). The hexagon depicts the first Brillouin zone. (c) Fourier transform of the numerical simulation of charge density variation. This figure is the same as Fig. S14(f) [49].

first term represents the conventional Kitaev interaction, and the second term is an enhancement in the negative bias. J_H is the Hund coupling, U is the on-site Coulomb repulsion, t is the hopping amplitude between neighboring sites, and t_S is the amplitude for the tunneling of the extra holes. On the other hand, such processes increasing the Kitaev interaction are absent for positive bias voltages. This prediction is confirmed by model calculations, which show that the difference of the Kitaev interaction between the negative and positive bias voltages is estimated as $(K_{\text{negative}} - K_{\text{positive}})/K \sim 0.0543 \sim 0.176$, where K is the Kitaev interaction without the corrections. The magnitude of the difference varies depending on the choice of parameters. As the Kitaev interaction increases, the ratio of scalar chirality to Kitaev interaction decreases, leading to smaller wave numbers, which explains the different wave numbers shown in Fig. 5(g). (The discussion in this paragraph is detailed in Supplemental Material F [49].)

While we have suggested the origin of the oscillation as described above, there may be different explanations [74], and a more comprehensive understanding is open for future research. Importantly, however, the decaying, incommensurate, and bias-semi-independent oscillation we found in the insulator manifests a new oscillatory phenomenon. The unforeseen oscillation represents the atomic-scale response of the quantum state with characteristic length scales. The absence of such oscillations in other Mott insulators and monolayer films implies that the observed oscillation may serve as a local signifier of the Kitaev QSL, which is experimentally elusive.

IV. METHODS

A. Sample fabrication

Monolayer α-$RuCl_3$ films were deposited on HOPG substrates by pulsed laser deposition using a yttrium-aluminium-garnet laser (wavelength 1064 nm). The targets were pelletized α-$RuCl_3$ single crystals grown by chemical

vapor transport from commercial $RuCl_3$ powder. The chlorine partial pressure and the substrate temperature were optimized at 2000 Pa and 430 °C. This condition is essential to grow the α phase separately from the β phase [75] without mixing the two phases [48]. The fabricated thin films were transferred from the deposition chamber to the STM chamber without air exposure using a portable ultrahigh vacuum chamber.

B. Spectroscopic-imaging scanning tunneling microscopy

Spectroscopic-imaging scanning tunneling microscopy measurements were performed using a low-temperature ultrahigh vacuum system (UNISOKU USM 1300). The scanning tips were mechanically sharpened Pt-Ir wires cleaned by electron-beam heating and conditioned on clean Au(111) surfaces. All the measurements were carried out at 5 K unless otherwise noted. Topographic images were recorded in the constant-current mode. Differential conductance spectra were measured using a standard lock-in technique with a modulation amplitude of 20 meV at a frequency of 973 Hz. The normalized conductance is obtained by numerical division. When Fourier transforms are calculated, affine transformations are applied as described in Supplemental Material D [49], and no symmetrization is used.

ACKNOWLEDGMENTS

The authors thank J. Knolle, E.-G. Moon, Y. Motome, J. Nasu, M. Udagawa, and M. G. Yamada for fruitful discussions. This work was supported by CREST (Grant No. JPMJCR19T5) from Japan Science and Technology (JST), and Grants-in-Aid for Scientific Research (KAKENHI) (Grants No. JP20K03860, No. JP21H01039, No. JP22J20066, No. JP22H00105, No. JP22H01221, No. JP23H00089, and No. JP23K17669) and Grant-in-Aid for Scientific Research on Innovative Areas "Quantum Liquid Crystals" (Grants No. JP19H05824, No. JP22H04480) from Japan Society for the Promotion of Science (JSPS). M. O. T. acknowledges support from a JSPS Fellowship for Young Scientists.

[1] J. Friedel, *The distribution of electrons round impurities in monovalent metals*, Philos. Mag. J. Sci. **43**, 153 (1952).
[2] J. Kondo, *Resistance minimum in dilute magnetic alloys*, Prog. Theor. Phys. **32**, 37 (1964).
[3] S. H. Pan, E. W. Hudson, K. M. Lang, H. Eisaki, S. Uchida, and J. C. Davis, *Imaging the effects of individual zinc impurity atoms on superconductivity in* $Bi_2Sr_2CaCu_2O_{8+\delta}$, Nature (London) **403**, 746 (2000).
[4] D. Kitchen, A. Richardella, J.-M. Tang, M. E. Flatté, and A. Yazdani, *Atom-by-atom substitution of* Mn *in* GaAs *and visualization of their hole-mediated interactions*, Nature (London) **442**, 436 (2006).
[5] S.-H. Ji, T. Zhang, Y.-S. Fu, X. Chen, X.-C. Ma, J. Li, W.-H. Duan, J.-F. Jia, and Q.-K. Xue, *High-resolution scanning tunneling spectroscopy of magnetic impurity induced bound states in the superconducting gap of* Pb *thin films*, Phys. Rev. Lett. **100**, 226801 (2008).
[6] L. Savary and L. Balents, *Quantum spin liquids: A review*, Rep. Prog. Phys. **80**, 016502 (2016).
[7] A. J. Willans, J. T. Chalker, and R. Moessner, *Disorder in a quantum spin liquid: Flux binding and local moment formation*, Phys. Rev. Lett. **104**, 237203 (2010).
[8] M. Vojta, A. K. Mitchell, and F. Zschocke, *Kondo impurities in the Kitaev spin liquid: Numerical renormalization group solution and gauge-flux-driven screening*, Phys. Rev. Lett. **117**, 037202 (2016).
[9] S. D. Das, K. Dhochak, and V. Tripathi, *Kondo route to spin inhomogeneities in the honeycomb Kitaev model*, Phys. Rev. B **94**, 024411 (2016).
[10] R. Wang, Y. Wang, Y. X. Zhao, and B. Wang, *Emergent Kondo behavior from gauge fluctuations in spin liquids*, Phys. Rev. Lett. **127**, 237202 (2021).
[11] A. Kolezhuk, S. Sachdev, R. R. Biswas, and P. Chen, *Theory of quantum impurities in spin liquids*, Phys. Rev. B **74**, 165114 (2006).
[12] P. Ribeiro and P. A. Lee, *Magnetic impurity in a* $U(1)$ *spin liquid with a spinon Fermi surface*, Phys. Rev. B **83**, 235119 (2011).
[13] D. F. Mross and T. Senthil, *Charge Friedel oscillations in a Mott insulator*, Phys. Rev. B **84**, 041102(R) (2011).
[14] H. Takagi, T. Takayama, G. Jackeli, G. Khaliullin, and S. E. Nagler, *Concept and realization of Kitaev quantum spin liquids*, Nat. Rev. Phys. **1**, 264 (2019).
[15] Y. Motome and J. Nasu, *Hunting Majorana fermions in Kitaev magnets*, J. Phys. Soc. Jpn. **89**, 012002 (2020).
[16] A. Kitaev, *Anyons in an exactly solved model and beyond*, Ann. Phys. (Amsterdam) **321**, 2 (2006).
[17] G. Jackeli and G. Khaliullin, *Mott insulators in the strong spin-orbit coupling limit: From Heisenberg to a quantum compass and Kitaev models*, Phys. Rev. Lett. **102**, 017205 (2009).
[18] K. W. Plumb, J. P. Clancy, L. J. Sandilands, V. V. Shankar, Y. F. Hu, K. S. Burch, H.-Y. Kee, and Y.-J. Kim, α-$RuCl_3$*: A spin-orbit assisted Mott insulator on a honeycomb lattice*, Phys. Rev. B **90**, 041112(R) (2014).
[19] R. D. Johnson, S. C. Williams, A. A. Haghighirad, J. Singleton, V. Zapf, P. Manuel, I. I. Mazin, Y. Li, H. O. Jeschke, R. Valentí, and R. Coldea, *Monoclinic crystal structure of* α-$RuCl_3$ *and the zigzag antiferromagnetic ground state*, Phys. Rev. B **92**, 235119 (2015).
[20] H.-S. Kim, Vijay Shankar V., A. Catuneanu, and H.-Y. Kee, *Kitaev magnetism in honeycomb* α-$RuCl_3$ *with intermediate spin-orbit coupling*, Phys. Rev. B **91**, 241110(R) (2015).
[21] H. B. Cao, A. Banerjee, J.-Q. Yan, C. A. Bridges, M. D. Lumsden, D. G. Mandrus, D. A. Tennant, B. C. Chakoumakos, and S. E. Nagler, *Low-temperature crystal and magnetic structure of* α-$RuCl_3$, Phys. Rev. B **93**, 134423 (2016).
[22] L. J. Sandilands, Y. Tian, K. W. Plumb, Y.-J. Kim, and K. S. Burch, *Scattering continuum and possible fractionalized excitations in* α-$RuCl_3$, Phys. Rev. Lett. **114**, 147201 (2015).

[23] J. Nasu, J. Knolle, D. L. Kovrizhin, Y. Motome, and R. Moessner, *Fermionic response from fractionalization in an insulating two-dimensional magnet*, Nat. Phys. **12**, 912 (2016).

[24] A. Banerjee, C. A. Bridges, J.-Q. Yan, A. A. Aczel, L. Li, M. B. Stone, G. E. Granroth, M. D. Lumsden, Y. Yiu, J. Knolle, S. Bhattacharjee, D. L. Kovrizhin, R. Moessner, D. A. Tennant, D. G. Mandrus, and S. E. Nagler, *Proximate Kitaev quantum spin liquid behaviour in a honeycomb magnet*, Nat. Mater. **15**, 733 (2016).

[25] A. Banerjee, J. Yan, J. Knolle, C. A. Bridges, M. B. Stone, M. D. Lumsden, D. G. Mandrus, D. A. Tennant, R. Moessner, and S. E. Nagler, *Neutron scattering in the proximate quantum spin liquid* α-$RuCl_3$, Science **356**, 1055 (2017).

[26] S.-H. Do, S.-Y. Park, J. Yoshitake, J. Nasu, Y. Motome, Y. S. Kwon, D. T. Adroja, D. J. Voneshen, K. Kim, T.-H. Jang, J.-H. Park, K.-Y. Choi, and S. Ji, *Majorana fermions in the Kitaev quantum spin system* α-$RuCl_3$, Nat. Phys. **13**, 1079 (2017).

[27] S. Widmann, V. Tsurkan, D. A. Prishchenko, V. G. Mazurenko, A. A. Tsirlin, and A. Loidl, *Thermodynamic evidence of fractionalized excitations in* α-$RuCl_3$, Phys. Rev. B **99**, 094415 (2019).

[28] O. Tanaka, Y. Mizukami, R. Harasawa, K. Hashimoto, K. Hwang, N. Kurita, H. Tanaka, S. Fujimoto, Y. Matsuda, E.-G. Moon, and T. Shibauchi, *Thermodynamic evidence for a field-angle-dependent Majorana gap in a Kitaev spin liquid*, Nat. Phys. **18**, 429 (2022).

[29] Y. Kasahara, T. Ohnishi, Y. Mizukami, O. Tanaka, S. Ma, K. Sugii, N. Kurita, H. Tanaka, J. Nasu, Y. Motome, T. Shibauchi, and Y. Matsuda, *Majorana quantization and half-integer thermal quantum Hall effect in a Kitaev spin liquid*, Nature (London) **559**, 227 (2018).

[30] M. Yamashita, J. Gouchi, Y. Uwatoko, N. Kurita, and H. Tanaka, *Sample dependence of half-integer quantized thermal Hall effect in the Kitaev spin-liquid candidate* α-$RuCl_3$, Phys. Rev. B **102**, 220404(R) (2020).

[31] T. Yokoi, S. Ma, Y. Kasahara, S. Kasahara, T. Shibauchi, N. Kurita, H. Tanaka, J. Nasu, Y. Motome, C. Hickey, S. Trebst, and Y. Matsuda, *Half-integer quantized anomalous thermal Hall effect in the Kitaev material candidate* α-$RuCl_3$, Science **373**, 568 (2021).

[32] J. A. N. Bruin, R. R. Claus, Y. Matsumoto, N. Kurita, H. Tanaka, and H. Takagi, *Robustness of the thermal Hall effect close to half-quantization in* α-$RuCl_3$, Nat. Phys. **18**, 401 (2022).

[33] P. Czajka, T. Gao, M. Hirschberger, P. Lampen-Kelley, A. Banerjee, N. Quirk, D. G. Mandrus, S. E. Nagler, and N. P. Ong, *Planar thermal Hall effect of topological bosons in the Kitaev magnet* α-$RuCl_3$, Nat. Mater. **22**, 36 (2022).

[34] Z. Zhu, P. A. Maksimov, S. R. White, and A. L. Chernyshev, *Disorder-induced mimicry of a spin liquid in* $YbMgGaO_4$, Phys. Rev. Lett. **119**, 157201 (2017).

[35] C. Balz, L. Janssen, P. Lampen-Kelley, A. Banerjee, Y. H. Liu, J.-Q. Yan, D. G. Mandrus, M. Vojta, and S. E. Nagler, *Field-induced intermediate ordered phase and anisotropic interlayer interactions in* α-$RuCl_3$, Phys. Rev. B **103**, 174417 (2021).

[36] R. G. Pereira and R. Egger, *Electrical access to Ising anyons in Kitaev spin liquids*, Phys. Rev. Lett. **125**, 227202 (2020).

[37] J. Feldmeier, W. Natori, M. Knap, and J. Knolle, *Local probes for charge-neutral edge states in two-dimensional quantum magnets*, Phys. Rev. B **102**, 134423 (2020).

[38] E. J. König, M. T. Randeria, and B. Jäck, *Tunneling spectroscopy of quantum spin liquids*, Phys. Rev. Lett. **125**, 267206 (2020).

[39] M. Udagawa, S. Takayoshi, and T. Oka, *Scanning tunneling microscopy as a single Majorana detector of Kitaev's chiral spin liquid*, Phys. Rev. Lett. **126**, 127201 (2021).

[40] S.-H. Jang, Y. Kato, and Y. Motome, *Vortex creation and control in the Kitaev spin liquid by local bond modulations*, Phys. Rev. B **104**, 085142 (2021).

[41] T. Bauer, L. R. D. Freitas, R. G. Pereira, and R. Egger, *Scanning tunneling spectroscopy of Majorana zero modes in a Kitaev spin liquid*, Phys. Rev. B **107**, 054432 (2023).

[42] W. Ruan, Y. Chen, S. Tang, J. Hwang, H.-Z. Tsai, R. L. Lee, M. Wu, H. Ryu, S. Kahn, F. Liou, C. Jia, A. Aikawa, C. Hwang, F. Wang, Y. Choi, S. G. Louie, P. A. Lee, Z.-X. Shen, S.-K. Mo, and M. F. Crommie, *Evidence for quantum spin liquid behaviour in single-layer* $1T$-$TaSe_2$ *from scanning tunnelling microscopy*, Nat. Phys. **17**, 1154 (2021).

[43] Y. Chen, W.-Y. He, W. Ruan, J. Hwang, S. Tang, R. L. Lee, M. Wu, T. Zhu, C. Zhang, H. Ryu, F. Wang, S. G. Louie, Z.-X. Shen, S.-K. Mo, P. A. Lee, and M. F. Crommie, *Evidence for a spinon Kondo effect in cobalt atoms on single-layer* $1T$-$TaSe_2$, Nat. Phys. **18**, 1335 (2022).

[44] L. Du, Y. Huang, Y. Wang, Q. Wang, R. Yang, J. Tang, M. Liao, D. Shi, Y. Shi, X. Zhou, Q. Zhang, and G. Zhang, *2D proximate quantum spin liquid state in atomic-thin* α-$RuCl_3$, 2D Mater. **6**, 015014 (2018).

[45] X. Zheng, K. Jia, J. Ren, C. Yang, X. Wu, Y. Shi, K. Tanigaki, and R.-R. Du, *Tunneling spectroscopic signatures of charge doping and associated Mott transition in* α-$RuCl_3$ *in proximity to graphite*, Phys. Rev. B **107**, 195107 (2023).

[46] X. Zheng, O. Takuma, H. Zhou, C. Yang, X. Han, G. Wang, J. Ren, Y. Shi, K. Tanigaki, and R.-R. Du, *Insulator-to-metal Mott transition facilitated by lattice deformation in monolayer* α-$RuCl_3$ *on graphite*, Phys. Rev. B **109**, 035106 (2024).

[47] K. Momma and F. Izumi, *VESTA for three-dimensional visualization of crystal, volumetric and morphology data*, J. Appl. Crystallogr. **44**, 1272 (2011).

[48] Z. Wang, L. Liu, H. Zheng, M. Zhao, K. Yang, C. Wang, F. Yang, H. Wu, and C. Gao, *Direct observation of the Mottness and p–d orbital hybridization in the epitaxial monolayer* α-$RuCl_3$, Nanoscale **14**, 11745 (2022).

[49] See Supplemental Material at http://link.aps.org/supplemental/10.1103/PhysRevX.14.041026 for Supplemental Figures and discussion including statistical analysis of apparent film thickness, local amplitude map of the decaying oscillation, excluding commensurate structures, how to calculate positions of satellite peaks, the lattice constant of α-$RuCl_3$ films, and Majorana-based scenario for the incommensurate spatial oscillation, which includes Refs. [50–56].

[50] Y. Kohsaka, *Removing background and estimating a unit height of atomic steps from a scanning probe microscopy*

image using a statistical model, Rev. Sci. Instrum. **92**, 033702 (2021).

[51] M. J. Lawler, K. Fujita, J. Lee, A. R. Schmidt, Y. Kohsaka, C. K. Kim, H. Eisaki, S. Uchida, J. C. Davis, J. P. Sethna, and E.-A. Kim, *Intra-unit-cell electronic nematicity of the high-T_c copper-oxide pseudogap states*, Nature (London) **466**, 347 (2010).

[52] Y. Baskin and L. Meyer, *Lattice constants of graphite at low temperatures*, Phys. Rev. **100**, 544 (1955).

[53] S. M. Winter, Y. Li, H. O. Jeschke, and R. Valentí, *Challenges in design of Kitaev materials: Magnetic interactions from competing energy scales*, Phys. Rev. B **93**, 214431 (2016).

[54] C. J. Morningstar and M. Weinstein, *Contractor renormalization group method: A new computational technique for lattice systems*, Phys. Rev. Lett. **73**, 1873 (1994).

[55] E. Altman and A. Auerbach, *Plaquette boson-fermion model of cuprates*, Phys. Rev. B **65**, 104508 (2002).

[56] S. Capponi, A. Läuchli, and M. Mambrini, *Numerical contractor renormalization method for quantum spin models*, Phys. Rev. B **70**, 104424 (2004).

[57] B. Yang, Y. M. Goh, S. H. Sung, G. Ye, S. Biswas, D. A. S. Kaib, R. Dhakal, S. Yan, C. Li, S. Jiang, F. Chen, H. Lei, R. He, R. Valentí, S. M. Winter, R. Hovden, and A. W. Tsen, *Magnetic anisotropy reversal driven by structural symmetry-breaking in monolayer α-$RuCl_3$*, Nat. Mater. **22**, 50 (2022).

[58] S. Mashhadi, Y. Kim, J. Kim, D. Weber, T. Taniguchi, K. Watanabe, N. Park, B. Lotsch, J. H. Smet, M. Burghard, and K. Kern, *Spin-split band hybridization in graphene proximitized with α-$RuCl_3$ nanosheets*, Nano Lett. **19**, 4659 (2019).

[59] B. Zhou, J. Balgley, P. Lampen-Kelley, J.-Q. Yan, D. G. Mandrus, and E. A. Henriksen, *Evidence for charge transfer and proximate magnetism in graphene–α-$RuCl_3$ heterostructures*, Phys. Rev. B **100**, 165426 (2019).

[60] D. J. Rizzo, B. S. Jessen, Z. Sun, F. L. Ruta, J. Zhang, J.-Q. Yan, L. Xian, A. S. McLeod, M. E. Berkowitz, K. Watanabe, T. Taniguchi, S. E. Nagler, D. G. Mandrus, A. Rubio, M. M. Fogler, A. J. Millis, J. C. Hone, C. R. Dean, and D. N. Basov, *Charge-transfer plasmon polaritons at graphene/α-$RuCl_3$ interfaces*, Nano Lett. **20**, 8438 (2020).

[61] Zhizhan Qiu, Yixuan Han, Keian Noori, Zhaolong Chen, Mikhail Kashchenko, Li Lin, Thomas Olsen, Jing Li, Hanyan Fang, Pin Lyu, Mykola Telychko, Xingyu Gu, Shaffique Adam, Su Ying Quek, Aleksandr Rodin, A. H. Castro Neto, Kostya S. Novoselov, and Jiong Lu, *Evidence for electron-hole crystals in a Mott insulator*, Nat. Mater. **23**, 1055 (2024).

[62] C. Price and N. B. Perkins, *Finite-temperature phase diagram of the classical Kitaev-Heisenberg model*, Phys. Rev. B **88**, 024410 (2013).

[63] Y. Imry and S.-k. Ma, *Random-field instability of the ordered state of continuous symmetry*, Phys. Rev. Lett. **35**, 1399 (1975).

[64] W. Jolie, J. Lux, M. Pörtner, D. Dombrowski, C. Herbig, T. Knispel, S. Simon, T. Michely, A. Rosch, and C. Busse, *Suppression of quasiparticle scattering signals in bilayer graphene due to layer polarization and destructive interference*, Phys. Rev. Lett. **120**, 106801 (2018).

[65] C. Ye, P. Cai, R. Yu, X. Zhou, W. Ruan, Q. Liu, C. Jin, and Y. Wang, *Visualizing the atomic-scale electronic structure of the $Ca_2CuO_2Cl_2$ Mott insulator*, Nat. Commun. **4**, 1365 (2013).

[66] J. Dai, E. Calleja, G. Cao, and K. McElroy, *Local density of states study of a spin-orbit-coupling induced Mott insulator Sr_2IrO_4*, Phys. Rev. B **90**, 041102(R) (2014).

[67] Z. Wu, K. Bu, W. Zhang, Y. Fei, Y. Zheng, J. Gao, X. Luo, Z. Liu, Y.-P. Sun, and Y. Yin, *Effect of stacking order on the electronic state of 1T-TaS_2*, Phys. Rev. B **105**, 035109 (2022).

[68] R.-F. Wang, J. Guan, Y.-L. Xiong, X.-F. Zhang, J.-Q. Fan, J. Zhu, C.-L. Song, X.-C. Ma, and Q.-K. Xue, *Electronic inhomogeneity and band structure in superstructural CuO_2 planes of infinite-layer $Sr_{0.94}La_{0.06}CuO_{2+y}$ films*, Phys. Rev. B **102**, 100508(R) (2020).

[69] W. Chen, Z. Sun, Z. Wang, L. Gu, X. Xu, S. Wu, and C. Gao, *Direct observation of van der Waals stacking–dependent interlayer magnetism*, Science **366**, 983 (2019).

[70] K. Quertite, H. Enriquez, N. Trcera, A. Bendounan, A. J. Mayne, G. Dujardin, A. El kenz, A. Benyoussef, Y. J. Dappe, A. Kara, and H. Oughaddou, *Electron beam analysis induces* Cl *vacancy defects in a* NaCl *thin film*, Nanotechnology **33**, 095706 (2021).

[71] L. N. Bulaevskii, C. D. Batista, M. V. Mostovoy, and D. I. Khomskii, *Electronic orbital currents and polarization in Mott insulators*, Phys. Rev. B **78**, 024402 (2008).

[72] D. Takikawa and S. Fujimoto, *Impact of off-diagonal exchange interactions on the Kitaev spin-liquid state of α-$RuCl_3$*, Phys. Rev. B **99**, 224409 (2019).

[73] K. Shiozaki, M. Sato, and K. Gomi, *Atiyah-Hirzebruch spectral sequence in band topology: General formalism and topological invariants for 230 space groups*, Phys. Rev. B **106**, 165103 (2022).

[74] K. Zhang, S. Feng, Y. D. Lensky, N. Trivedi, and E.-A. Kim, *Machine learning reveals features of spinon Fermi surface*, Commun. Phys. **7**, 54 (2024).

[75] T. Asaba, L. Peng, T. Ono, S. Akutagawa, I. Tanaka, H. Murayama, S. Suetsugu, A. Razpopov, Y. Kasahara, T. Terashima, Y. Kohsaka, T. Shibauchi, M. Ichikawa, R. Valentí, S.-I. Sasa, and Y. Matsuda, *Growth of self-integrated atomic quantum wires and junctions of a Mott semiconductor*, Sci. Adv. **9**, eabq5561 (2023).